



# Hydrothermal synthesis of nitrogen-doped graphene quantum dots as a fluorescent probe to detect mercury (II) ions in an aqueous sample

Anis Sofia Awalludin<sup>1</sup> · Pravena Ramachandran<sup>1</sup> · Purim Jarujamrus<sup>2,3</sup> · Hooi Ling Lee<sup>1</sup>

Received: 27 December 2021 / Accepted: 10 February 2022 / Published online: 4 March 2022  
© Qatar University and Springer Nature Switzerland AG 2022

## Abstract

The N-doped graphene quantum dots (N-GQDs) with a high quantum yield of 36.23% were synthesised through a facile hydrothermal method by using citric acid monohydrate (CA) and ethylenediamine (EDA) as the carbon and nitrogen precursors, respectively. The morphology and the surface functional group of N-GQDs were analysed by using Fourier transform infrared (FTIR) spectroscopy and high-resolution transmission electron microscopy (HRTEM) while the optical properties were observed with UV–Vis spectroscopy and photoluminescence spectroscopy (PL). The synthesised N-GQDs were reported to form in a spherical shape with an average particles size of  $9.96 \pm 4.4$  nm based on the HRTEM analysis. Furthermore, the as-prepared N-GQDs emitted a bright blue fluorescence emission with an excitation-independent fluorescence emission at 440 nm with the excitation wavelength at 340 nm. Linear regression between fluorescence intensity and  $\text{Hg}^{2+}$  ions at different concentrations was obtained and the limit of detection (LOD) and the limit of quantification (LOQ) were calculated as 2.46  $\mu\text{M}$  and 7.45  $\mu\text{M}$ , respectively. In addition, the fluorescence quenching effect that occurs in the interaction between  $\text{Hg}^{2+}$  ions and N-GQDs corresponded to the dynamic quenching mechanism. The higher selectivity towards  $\text{Hg}^{2+}$  ions proved that this synthesised N-GQDs could be used as a fluorescent probe to detect  $\text{Hg}^{2+}$  ions in an aqueous solution.

**Keywords** N-doped graphene quantum dots · Hydrothermal synthesis · Fluorescent probe · Dynamic quenching · Mercury ions detection

## 1 Introduction

Mercury ions ( $\text{Hg}^{2+}$ ) are one of the heavy metal ions that have threatened aquatic and human health due to their strong toxicity [1, 2]. According to Yang and his co-workers, mercuric ions can bring higher health risks to living organisms even in low concentrations, which are within 5 ppb (0.025  $\mu\text{M}$ ) [3]. Usually,  $\text{Hg}^{2+}$  ions were disposed into the aquatic environment from some manufacturing industries that lead to the improper discharge of industrial wastewater

or domestic effluents [4, 5] and daily household water [6]. The uncontrolled disposal of  $\text{Hg}^{2+}$  ions in water can cause pollution and trigger poisoning events in humans [7, 8]. Besides, the bio-accumulation of  $\text{Hg}^{2+}$  ions can react with the protein's sulfhydryl group in the human organ which can cause severe human health problems like kidney failure, brain damage, and a neurological disorder [9, 10]. In this regard, it is crucial to develop a method that is highly selective and sensitive for  $\text{Hg}^{2+}$  ions detection in an aqueous solution.

In the past few years, inductive coupled plasma mass spectroscopy (ICP-MS) [11, 12], atomic absorption or atomic emission spectroscopy (AAS/AES) [13], atomic fluorescence spectrometry (AFS) [14], and high-performance liquid chromatography (HPLC) [15] was widely used as an analytical method for  $\text{Hg}^{2+}$  ions detections. Then, recently several new methods have been introduced for  $\text{Hg}^{2+}$  ions detection based on intrinsic catalytic performance which is using nanoparticles and nanoenzyme [16–21]. The reports of previous research on various methods for  $\text{Hg}^{2+}$  ions determination were listed in Table 1.

✉ Hooi Ling Lee  
hllee@usm.my

<sup>1</sup> Nanomaterials Research Group, School of Chemical Sciences, Universiti Sains Malaysia, Penang, Malaysia

<sup>2</sup> Department of Chemistry and Centre of Excellence for Innovation in Chemistry, Faculty of Science, Ubon Ratchathani University, Ubon Ratchathani, Thailand

<sup>3</sup> Nanomaterials Science, Sensors & Catalysis for Problem-Based Projects, Faculty of Science, Ubon Ratchathani University, Ubon Ratchathani, Thailand

**Table 1** Detection of Hg<sup>2+</sup> ions using various methods

Methods	Samples	LOD (μM)	References
Magnetic solid-phase extraction (MSPE)-HPLC-ICP-MS	Fish samples and water	$3.7 \times 10^{-6}$	[12]
Cold vapour atomic absorption spectrometry (AAS)	Fish samples and water	$5.0 \times 10^{-5}$	[13]
Ultraviolet atomisation-atomic fluorescence (UV-AFS)	Water	0.075	[14]
Calorimetric method by using molybdenum disulfide nanosheet	Cosmetic samples	0.5	[18]
Calorimetric method by using manganese oxide nanorods	Real water samples	0.08	[19]
Membrane-based calorimetric sensor	Water	15	[20]
Surface-enhanced Raman scattering by using modified silver nanoparticles (Ag NPs)	Spiked water samples	0.0024	[21]
Photoluminescence Spectrometry by using N-doped graphene quantum dots (N-GQDs)	Spiked water samples	2.46	This work

As summarised in Table 1, all methods have shown excellent selectivity and sensitivity towards Hg<sup>2+</sup> ions. However, they use expensive equipment, complicated procedures in terms of instrumental hyphenation and sample preparation which lead to time-consuming. Therefore, the fluorescence detection method is preferable because it is more sensitive as the fluorescence intensity will directly change when the collision quenching between the analytes occurs. Besides, this method is also easy to operate and cost-effective.

In previously reported researches, numerous materials were used as the fluorescent probe in the detection of metal ions such as organic dyes [22], conjugated polymers [23], carbon dots [24], and others. Among them, inorganic semiconductor quantum dots (QDs) such as CdS, CdSe, and PbSe have been extensively used as fluorescent probes to detect Hg<sup>2+</sup> ions based on fluorescence quenching techniques [24, 25]. For instance, Haibing Li and co-workers have fabricated luminescent and stable CdSe/ZnS core quantum dots (QDs) capped with L-carnitine for Hg<sup>2+</sup> ions detection with a limit of detection (LOD) of  $1.8 \times 10^{-7}$  M [25]. However, some reports claimed that these QDs have higher toxicity and could not be employed in real environment applications [2, 10]. Due to these limitations, graphene quantum dots (GQDs) have been introduced as an environmentally friendly fluorescent probe and possess excellent photoluminescence properties, lower toxicity, and good biocompatibility. In addition, it has been reported that the surface modification of GQDs could easily be managed by tuning their fluorescence intensity for better detection of metal ions [26].

However, bare GQDs and modified surface GQDs do not have good selectivity for some target ions and the quantum yield is quite low. Therefore, to overcome this drawback, surface functionalisation and heteroatoms doping (e.g., nitrogen (N), boron (B), and sulfur (S)) on GQDs have been introduced [27–29]. This doping process reportedly can increase the quantum yield and enhance the fluorescence intensity by tuning the intrinsic properties [30]. The extra lone pair of electrons on the dopants will regulate the electron decolonisation by changing the charge distribution and tuning the energy bandgaps to improve the function of

GQDs. A study has reported that the nitrogen (N) atom is the preferred atom doped with GQDs because it has a similar atomic size to carbon and has a higher electronegativity than carbon [31]. Furthermore, it has been stated that the nitrogen would create three different bonding within the GQDs structure which are graphitic N, pyridinic N, and pyrrolic N that could affect the fluorescence properties of N-GQDs [32]. In addition, Ma and co-workers stated that N-doped GQDs would give a higher quantum yield and showed excellent fluorescence quenching performance than S-doped GQDs due to the pyridine N structure in N-GQDs [33]. Hence, N-doped GQDs are expected to produce a higher quantum yield with excellent fluorescence quenching performance.

N-GQDs can be synthesised by using two approaches which are top-down and bottom-up approaches. According to Ruili Liu and co-workers, the bottom-up approach is preferable compared to the other approach because it can easily control the size and the shape of N-GQDs [34]. Several methods can be classified as the bottom-up approach which are microwave, hydrothermal, thermal decomposition, pyrolysis, or carbonisation methods [35, 36]. Among these methods, the facile hydrothermal synthesis method is preferable to synthesise N-GQDs with a higher quantum yield because it has a simple procedure, low cost, and is environmentally friendly compared to other methods [9, 37–39]. A such, Fei Lu and co-workers have reported that a strong blue fluorescence of N-GQDs with a high quantum yield could be synthesised through a facile one-pot hydrothermal synthesis with citric acid (CA) and ethylenediamine (EDA) as carbon and nitrogen sources, respectively [40].

In addition, the quenching mechanism between the N-GQDs and Hg<sup>2+</sup> ions also plays an important role in the detection process. According to Fanlin Zu and co-workers, there are several types of quenching mechanisms that have been reported, which are static quenching, dynamic quenching, inner filter effect, photoinduced electron transfer (PET), and Förster resonance energy transfer (FRET) [41]. All these quenching mechanisms reported can influence the selectivity and sensitivity of N-GQDs toward metal ion detections [33, 41]. Previous studies stated that the quenching mechanism

could be identified by carrying out several experiments related to the absorbance, emission, and excitation spectrum [41, 42]. Therefore, the possible quenching mechanism that occurs between N-GQDs and  $\text{Hg}^{2+}$  ions could be further explored in this work.

Hence, in this study, N-GQDs were synthesised by using a facile and cost-effective technique which is hydrothermal synthesis by using a commonly available carbon and nitrogen precursor which is citric acid (CA) and ethylenediamine (EDA), respectively. These N-GQDs were used as a fluorescence probe to detect  $\text{Hg}^{2+}$  ions in the  $\text{Hg}^{2+}$  ions spiked real water samples. Furthermore, several characterisations were conducted on the N-GQDs to study morphology, composition, and other optical properties. The quenching mechanism was also studied by undergoing several tests on the absorbance and emission/excitation spectrum between N-GQDs and  $\text{Hg}^{2+}$  ions.

## 2 Experimental

### 2.1 Materials and chemicals

Citric acid monohydrate was obtained from Bendosen, Laboratory Chemicals (Malaysia), ethylenediamine QREC, Grade AR (Asia) Sdn. Bhd (Malaysia). Mercury (II) chloride, aluminium nitrate nanohydrate, iron(II) nitrate nonahydrate, magnesium chloride, cadmium chloride, and sodium hydroxide pellets were purchased from Merck KGaA (Germany). Calcium chloride, ammonium persulfate, and sodium chloride were purchased from Bendosen, Laboratory Chemicals (Malaysia). Nickel (II) chloride and phosphate buffer saline were purchased from Sigma-Aldrich, Co. (Germany). Lead (II) nitrate and sulphuric acid, 95–97% were purchased from QREC (Asia) Sdn. Bhd. (Malaysia). Copper (II) sulphate R&M Chemicals (UK). Hydrochloric acid, 37%, was purchased from RCI Labscan (Asia Pacific) Sdn. Bhd. Quinine sulphate dihydrate, 99%, was purchased from Across Organics (USA). All chemicals were of analytical grade without further purification.

### 2.2 Preparation of N-GQDs

The N-GQDs were synthesised via hydrothermal method using citric acid (CA) and ethylenediamine (EDA) as the carbon and nitrogen precursors. The synthesis method was directly executed from previously reported work [37]. Firstly, 1 mol of CA and 1 mol of EDA were dissolved in 5 mL of ultrapure water and stirred until the clear solution formed. Then, the solution was transferred into 20-mL Teflon-lined stainless-steel autoclaved and placed in the oven to undergo the hydrothermal treatment at 180 °C for 4 h. Finally, the black-brown transparent prepared sample

solution was centrifuged at 5000 rpm for 5 min to obtain purified liquid N-GQDs.

### 2.3 Characterisations

The optical characterisation was conducted using LAMBDA 25 UV–Visible Spectrophotometer (Shimadzu, Japan) at the wavelength range of 200–800 nm and PERKIN ELMER LS 55 Luminescence Spectrometer (USA) at a wavelength range of 300–700 nm to determine the absorption spectra and the fluorescence properties of synthesised N-GQDs, respectively. Fourier Transform Infrared (FTIR) spectrum of the synthesised sample was analysed by the ATR technique on PerkinElmer Frontier FT-NIR Spectrometer Frontier (USA) in the range of 600–4000  $\text{cm}^{-1}$ . The morphology and particle size of synthesised N-GQDs were determined by using high-resolution transmission electron microscope (HRTEM) 200 kV with Field Emission, TECNAI G2 20 S-TWIN, FEI (Spain).

### 2.4 Quantum yield (QY) measurement of N-GQDs

The quantum yield (QY) of N-GQDs was measured using a quinine sulfate in 0.1 M of  $\text{H}_2\text{SO}_4$  as a standard [43]. In this part, the absorbance and fluorescence intensity for five different concentrations of N-GQDs in ultrapure water and quinine sulfate in  $\text{H}_2\text{SO}_4$  were recorded. Based on the data, a graph of fluorescence intensity against absorbance containing two linear curves for both solutions has been plotted. Then, the QY of N-GQDs ( $Q_x$ ) was calculated at the excitation wavelength of 340 nm by using the following equation:

$$Q_x = Q_{st} \left( \frac{M_x}{M_{st}} \right) \left( \frac{\eta_x}{\eta_{st}} \right) \quad (1)$$

where,

Quantum yield of quinine sulfate: ( $Q_{st} = 0.54$ )

Refractive index of quinine sulfate: ( $\eta_{st} = 1.33$ )

Refractive index of N-GQDs: ( $\eta_x = 1.33$ )

### 2.5 Detection of mercury ions ( $\text{Hg}^{2+}$ )

The detection of  $\text{Hg}^{2+}$  ions was conducted in a neutral solution with phosphate-buffered saline (PBS) for 15 min at room temperature. An optimum excitation wavelength of 340 nm was used for the determination of fluorescence intensity by using a Perkin Elmer LS 55 Luminescence Spectrometer (USA). To determine the concentration of the  $\text{Hg}^{2+}$  ions that can be detected by N-GQDs, different concentrations were spiked into the N-GQDs solution.

A 10- $\mu\text{L}$  of N-GQDs was added into five 10-mL volumetric flasks. Then, five different concentrations of  $\text{Hg}^{2+}$  ions (5,

10, 15, 20, and 25  $\mu\text{M}$ ) from the stock solution are added to the five flasks, respectively. The final volume of 10 ml was topped up with a neutral solution of pH 7 (PBS). After 15 min, the fluorescence spectra were obtained. Lastly, a calibration curve was plotted between the fluorescence intensity at 440 nm ( $I_0/I$ ) against  $\text{Hg}^{2+}$  ions concentration, where  $I$  and  $I_0$  are the fluorescence intensity in the presence and absence of  $\text{Hg}^{2+}$  respectively. The calibration curve obtained will be used to calculate the limit of detection (LOD) and limit detection of quantification (LOQ) by using the following equation:

$$\text{LOD} = 3.3 * \text{SD}_{\text{blank}} / \text{slope} \quad (2)$$

$$\text{LOQ} = 10 * \text{SD}_{\text{blank}} / \text{slope} \quad (3)$$

In addition, an intra-day and inter-day precision of the fluorescence intensity was conducted for the five different concentrations of  $\text{Hg}^{2+}$  solutions (5, 10, 15, 20, 25  $\mu\text{M}$ ). For the intra-day precision, three fluorescence intensity reading for every concentration was collected five times in one day. Meanwhile, for inter-day precision, the fluorescence intensity reading was collected for five consecutive days. Besides, to determine the accuracy of  $\text{Hg}^{2+}$  ions detection by N-GQDs, the percentage recovery was calculated for three different concentrations of  $\text{Hg}^{2+}$  ions (15, 20 and 25  $\mu\text{M}$ ).

The effect of some parameters such as incubation time and pH solution was studied to determine the optimum incubation time and pH to detect  $\text{Hg}^{2+}$  in water. The experimental for these effect parameters will be explained in the supplementary information.

## 2.6 Selectivity of N-GQDs towards other metal ions

The selectivity of the N-GQDs towards other ions is tested to prove the  $\text{Hg}^{2+}$  ions are the most sensitive compared to other ions. To evaluate the selectivity, 25  $\mu\text{L}$  of various environmentally metal ions such as  $\text{Fe}^{3+}$ ,  $\text{Ca}^{2+}$ ,  $\text{Cd}^{2+}$ ,  $\text{Cu}^{2+}$ ,  $\text{Mg}^{2+}$ ,  $\text{Pb}^{2+}$ ,  $\text{Ni}^{2+}$ ,  $\text{Na}^+$ ,  $\text{Li}^+$ ,  $\text{Al}^{3+}$ , and  $\text{Hg}^{2+}$  ions was added into the 10-mL volumetric flask, separately. Then, 10  $\mu\text{L}$  of N-GQDs solution was added into the flask, and the final volume of 10 mL was adjusted with a solution of pH 7. The fluorescence spectra of each metal ion were recorded after 15 min. A triplicate measurement was obtained for each metal ion to get an average fluorescence intensity value with added ions assigned as  $I$ . A graph of the difference between blank fluorescence intensity and fluorescence intensity at 440 nm of added  $\text{Hg}^{2+}$  ions ( $I_0 - I$ ) against types of ions was plotted.

## 2.7 Determination of possible quenching mechanism of N-GQDs to $\text{Hg}^{2+}$ ions

### 2.7.1 Static and dynamic quenching mechanism

Based on the Stern Volmer relationship, a graph of  $I_0/I$  against the concentration of  $\text{Hg}^{2+}$  ions in N-GQDs solution was plotted to determine the type of quenching mechanism is static or dynamic. Five concentration was tested in this experiment, which is 5, 10, 15, 20, and 25  $\mu\text{M}$ . A linear plot of  $I_0/I$  against the concentration of  $\text{Hg}^{2+}$  ions indicates there is dynamic quenching. Meanwhile, if the graph shows the upward plot indicates the combination of static and dynamic quenching mechanisms [44].

A calibration curve with linear regression with three different temperatures (25°, 40 °C, and 60 °C) was plotted for further confirmation. If the slope increases as the temperature increases, the dynamic quenching could be assigned as the existing quenching mechanism meanwhile, if the slope decrease, it could be assigned as static quenching.

Finally, the UV–Vis spectra of N-GQDs unspiked and spiked  $\text{Hg}^{2+}$  ions in N-GQDs (25  $\mu\text{M}$ ) were obtained to determine the change in the spectra. The spectra of spiked  $\text{Hg}^{2+}$  ions (25  $\mu\text{M}$ ) in N-GQDs have been collected within 5 min intervals at 0, 5, 10, and 15 min. All the spectra in the range of 200–800 nm were compared to observe the significant changes. If there are no changes, it will indicate a dynamic quenching. However, if the change is observed, it will indicate as a static quenching mechanism.

### 2.7.2 Inner filter effect quenching mechanism

Firstly, the absorbance of N-GQDs and  $\text{Hg}^{2+}$  ions at pH 7 was obtained. Then, it is followed by the fluorescence excitation and emission wavelength of N-GQDs. Next, the absorbance spectrum of N-GQDs and  $\text{Hg}^{2+}$  ions was plotted to ascertain whether there is an overlap in the absorbance spectrum. Then, the plotted graph was compiled with the data of fluorescence excitation and emission wavelength in one analysis graph. The inner filter effect quenching mechanism exists when the spectra overlap with each other [45].

## 2.8 Real sample analysis

The real water samples analysis was executed using mineral water obtained from a convenience store and tap water from our laboratory. These samples were filtered through a 0.2- $\mu\text{m}$  membrane. Then, the fluorescence intensity of N-GQDs in tap and mineral water in the absence of  $\text{Hg}^{2+}$  ions was recorded. Next, the unknown concentrations of  $\text{Hg}^{2+}$  ions were calculated by using an equation obtained on a plotted calibration curve of the fluorescence intensity at 440 nm ( $I_0/I$ ) against  $\text{Hg}^{2+}$  ions concentration, where  $I$  and  $I_0$  are



the fluorescence intensity in the presence and absence of  $\text{Hg}^{2+}$  ions respectively. Then, the recovery percentage of  $\text{Hg}^{2+}$  ions in real samples was calculated by spiking various concentrations of  $\text{Hg}^{2+}$  ions (5  $\mu\text{M}$ , 15  $\mu\text{M}$ , and 25  $\mu\text{M}$ ) into the tap water and mineral water.

### 3 Result and discussions

#### 3.1 Optical properties

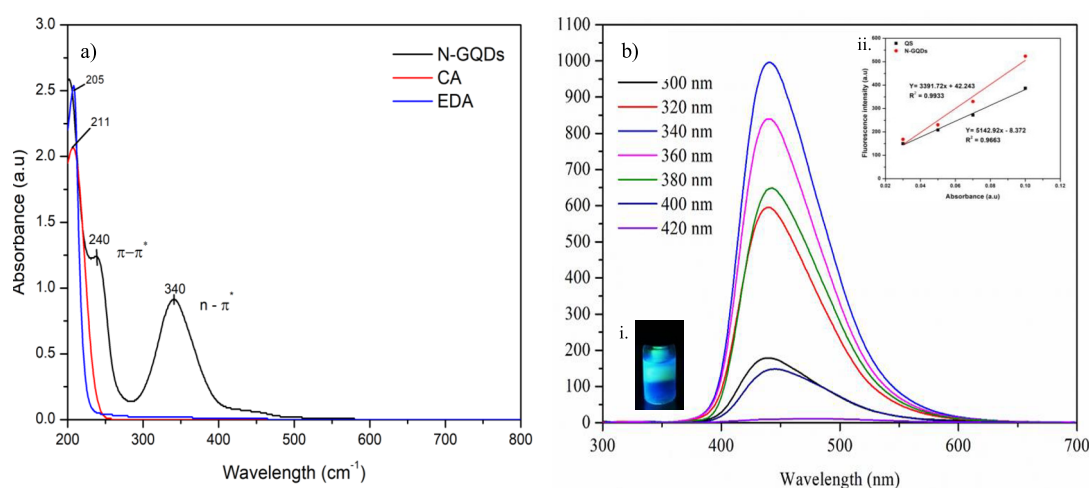
The optical properties of N-GQDs were determined by the UV–Vis absorption and fluorescence spectrum. Figure 1a illustrated the UV–Vis absorption spectrum of citric acid (CA), ethylenediamine (EDA), and synthesised N-GQDs. CA and EDA showed a single peak at 211 nm and 205 nm, respectively. The peak in CA corresponded to the carbonyl (C=O) group of the ionised or unionised carboxyl group, while the peak in EDA attributed to the amino group [46]. Meanwhile, there are two absorption peaks shown in the N-GQDs spectrum at 240 nm and 340 nm, respectively. The peak at 240 nm usually was assigned as the  $\pi$ - $\pi$  transition of aromatic  $\text{sp}^2$  domain, or to be specific, it is a transition of C=C double bond [40]. Then, a strong UV–Vis absorption peak at 340 nm is due to the  $n$ - $\pi^*$  shift of C=O and C-N [37, 47, 48]. Usually, the peak of the  $n$ - $\pi^*$  transition will be assigned as the excitation wavelength of fluorescence spectra because it can generate a strong photoluminescence emission. In contrast, the peak of  $\pi$ - $\pi$  will not generate any fluorescence emission [29, 46].

Figure 1b depicts the fluorescence spectra of synthesised N-GQDs using various excitation wavelengths (300, 320, 340, 360, 380, 400, and 420 nm). It showed that the

N-GQDs exhibit the excitation-independent fluorescence spectrum because the fluorescence peaks of N-GQDs did not shift as the excitation wavelength increased from 300 to 420 nm at a fluorescence emission of 440 nm. Generally, the excitation-independent of N-GQDs occurs due to the uniform size and the surface state of the  $\text{sp}^2$  clusters in the synthesised N-GQDs [50]. Furthermore, we can conclude that 340 nm is the optimum excitation wavelength because at that wavelength, N-GQDs emitted the maximum fluorescence intensity compared to other excitation wavelengths. The inset of Fig. 1b, (i) shows that N-GQDs emitted bright blue fluorescence under the 365 nm UV light. According to Tran Van Tam and co-workers, the intense bright blue fluorescence colour exhibited due to the higher electron affinity of the N atom doped on the pyridinic sites of N-GQDs could increase the quantum yield [38]. The quantum yield was calculated from the gradient of a linear relationship between the fluorescence intensity and absorbance of quinine sulphate and synthesised N-GQDs, shown in inset Fig. 1b, ii. As a result, the QY of as-synthesised N-GQDs is 36.23%, significantly higher than the other reported works via hydrothermal synthesis [27, 38].

#### 3.2 High-resolution transmission electron microscopy (HRTEM)

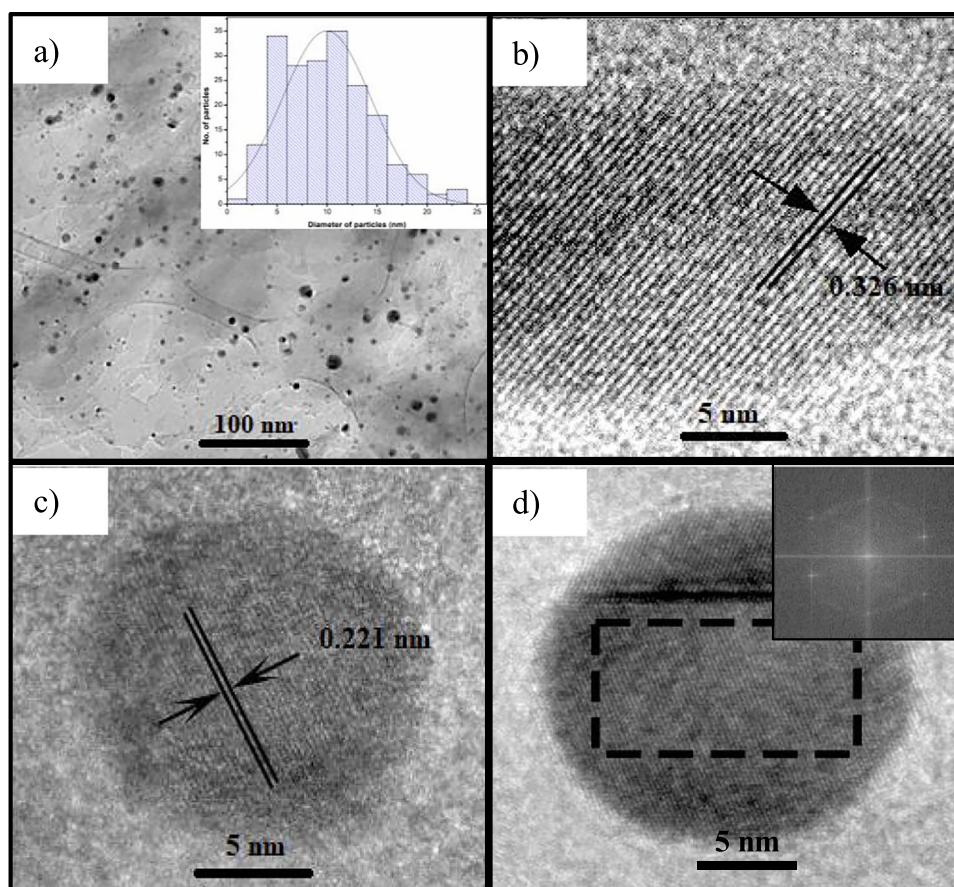
HRTEM analysis was employed to review the morphology structure and measure the particle size of obtained N-GQDs. The HRTEM images showed clear lattice fringes that attributed to the existence of high crystalline quality of N-GQDs. From Fig. 2a, the spherical quantum dots were uniformly distributed with a  $9.96 \pm 4.5$  nm average. Two hundreds of N-GQDs particles were randomly selected to calculate the



**Fig. 1** (a) UV–Vis spectra of citric acid, ethylenediamine and N-GQDs. (b) Fluorescence emission spectra of N-GQDs under different excitation wavelengths after being dispersed in ultra-pure water.

The inset (i) is an image of the diluted N-GQDs under the 365 nm UV light, (ii) Fluorescence intensity against UV–Vis absorbance of N-GQDs and quinine sulphate as the reference

**Fig. 2** (a)–(d) The HRTEM images of N-GQDs. The inset of (a) shows the particle size distribution of N-GQDs while inset of (d) shows the FFT image of a selected area of N-GQDs



average particle size, and from the particles distribution histogram (inset of Fig. 2a) there are some of the particle sizes of N-GQDs are higher than 10 nm could be due to the agglomeration during the drying process of the sample. Figure 2b and c are the particle's close-up images that indicate the crystalline structure of synthesised N-GQDs with lattice fringes of 0.326 nm and 0.221 nm, which indicates the formation of GQDs [51]. The presence of N-doping in the GQDs is further confirmed in the FTIR analysis as shown in the supplementary information (see Fig. S1 and Table S1). Furthermore, the further justification of the graphene quantum dots shown by the FFT image (inset of Fig. 2d) suggested the presence of hexagonal structure at the selected area of the HRTEM image.

### 3.3 Possible formation mechanism

In this work, the N-GQDs were synthesised by using citric acid and ethylenediamine as a precursor via hydrothermal synthesis. This bottom-up approach executed several processes like ionisation, condensation, polymerisation, and graphitisation, which has been reported by a few groups researchers [37, 49, 50, 52]. First, the ionisation process occurred when the CA and EDA transformed to their salts

containing  $\text{COO}^-$  and  $\text{NH}_2^+$  after added ultrapure water. Then, followed by the condensation process to produce a polymer-like structure of quantum dots. The increasing temperature in this reaction resulted in the formation of the N-doped carbon quantum dots, and then the graphitisation will take place and lead to the formation of N-GQDs. During graphitisation, the graphitic N would be substituted into the inner surface of the graphene hexagonal ring. Meanwhile, the pyrrolic N and pyridine N at the edge of the structure would hybridised to form a bond with C in the five-membered and six-membered rings, respectively [53]. Figure 3 illustrates the schematic chemical reaction of N-GQDs using citric acid monohydrate and ethylenediamine.

In addition, N-doping is preferred because it is not only preserved the primary properties of GQDs such as large specific surface area, quantum size effect, and good biocompatibility, but also gives distinctive optical and electronic features. The electron delocalisation and charge-carrier density of N-CDs can be significantly modified by tuning N-doping degree, C–N configurations, or surface functional groups. These characteristics are prone to provide N-GQDs with a better prospect as a probe [54, 55]. Hence, N-GQDs would inherit carboxyl, carbonyl, amino, amide, and hydroxyl groups from their precursors.

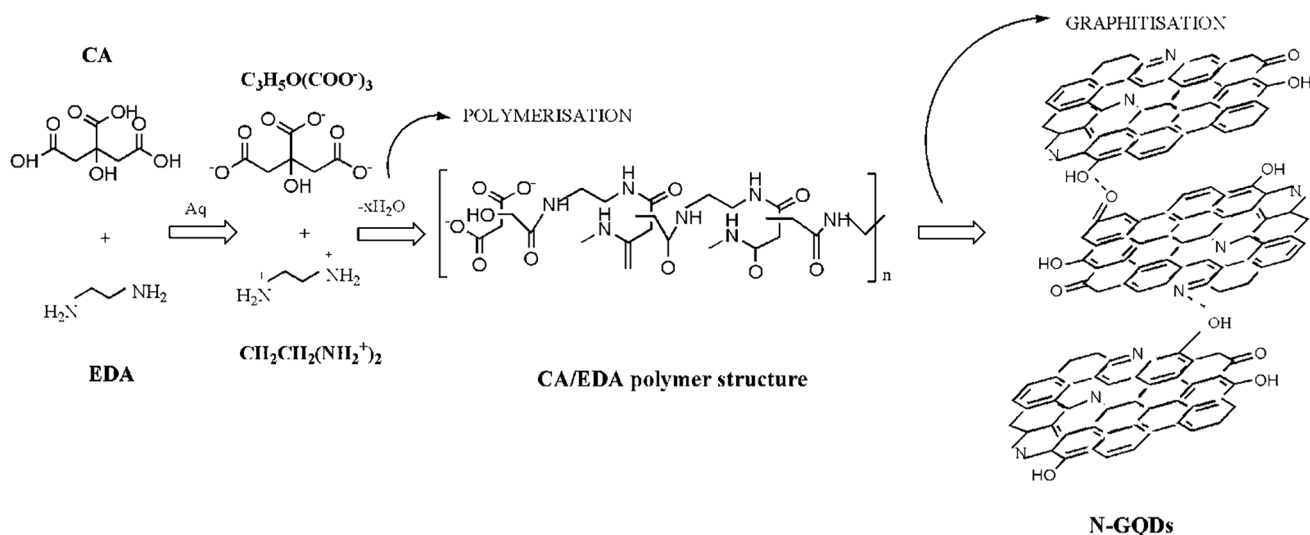


**Fig. 3** Schematic chemical reaction of N-GQDs using citric acid monohydrate and ethylenediamine

### 3.4 Determination of mercury ions ( $\text{Hg}^{2+}$ )

#### 3.4.1 Effect of incubation time and pH

It is crucial to observe the effect of incubation time and pH on the changes in the fluorescence intensity of N-GQDs to understand the quenching effect of the  $\text{Hg}^{2+}$  ions towards N-GQDs. Therefore, to study the effect of incubation time, the difference of fluorescence intensity ( $I_0 - I$ ) of N-GQDs was recorded for every one minute, and from the data plotted in Fig. S2a (see supplementary information), it is clearly shown that the changes in fluorescence intensity increased until it reached a constant reading at 15 min onwards as the time increased. The constant reading indicates that the N-GQDs have reached their maximum quenching effect. Therefore, 15 min was selected as the optimum incubation time for the detection of  $\text{Hg}^{2+}$  ions.

In order to study the effect of pH, the fluorescence intensity of N-GQDs was recorded at different pH values (pH 2–10). From Fig. S2b (see supplementary information), it could be observed that fluorescence intensities are quenched evidently from pH 2 until 7 and decreased as the pH increased from pH 8 to 10. The changes in the fluorescence intensities can be attributed to the protonation and deprotonation of the carboxyl group that presents at the surface of N-GQDs in alkaline and acidic conditions [49]. In the acidic state, the protonation of the carboxyl group would occur, and it would reduce the carboxyl group on the N-GQDs surface. As a result, there would be a weaker quenching effect due to the small reaction surface of  $\text{Hg}^{2+}$  ions on the N-GQDs. Meanwhile, at higher alkaline conditions, the deprotonation of the carboxyl group would lead to the other complex formation which is the  $\text{Hg}^{2+}$  ions

will react with the hydroxyl group instead of the carboxyl group. This could reduce the amount of  $\text{Hg}^{2+}$  ions that can react with synthesised N-GQDs and resulting in a lower quenching effect of the N-GQDs. The obtained finding clearly shows the highest quenching occurs at pH 7. Thus, the detection of  $\text{Hg}^{2+}$  ions by using fluorescence N-GQDs was executed in pH 7.

#### 3.4.2 Detection of $\text{Hg}^{2+}$ ions

The detection of  $\text{Hg}^{2+}$  ions was analysed by plotting the calibration curve and calculating the limit of detection (LOD) and limit of quantification (LOQ). The calibration curve obtained (Fig. S3, see supplementary information) shows a linear regression equation,  $y = 0.00608x + 0.9652$ , with an excellent linear correlation ( $R^2$ ) of 0.99117 as the concentration of  $\text{Hg}^{2+}$  ions increased from 5 to 25  $\mu\text{M}$ . This linear trend line indicates that the synthesised N-GQDs can function as a fluorescence probe to detect  $\text{Hg}^{2+}$  ions. Furthermore, from this analysis, the LOD and LOQ values were calculated to be 2.46  $\mu\text{M}$  and 7.45  $\mu\text{M}$ , respectively.

In addition, the intra-day and inter-day precision analyses were performed to determine the accuracy and precision of detecting  $\text{Hg}^{2+}$  ions by N-GQDs. The tabulated data in Table S2 (see supplementary information) shows the precision of the intra-day and intra-day analysis has a low (RSD) for the five different  $\text{Hg}^{2+}$  ions concentrations. Furthermore, the average percentage recovery also depicts the values of less than 100%, which indicates there is a good accuracy and precision of the detection of  $\text{Hg}^{2+}$  ions. Thus, this result has proven that the N-GQDs have excellent efficiency as a fluorescent probe for detecting  $\text{Hg}^{2+}$  ions.

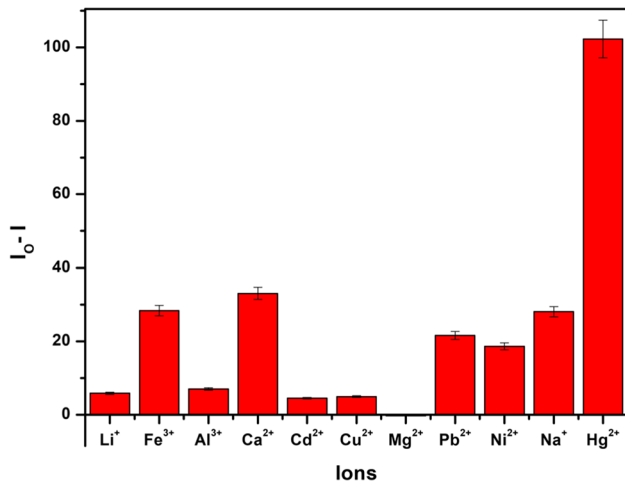


**Fig. 4** The selectivity of N-GQDs in the presence of various interfering cations at 25  $\mu\text{M}$  ( $n=3$ )

### 3.5 Selectivity of N-GQDs towards other ions

The selectivity of the N-GQDs was determined by adding various interfering metal cations such as  $\text{Fe}^{3+}$ ,  $\text{Ca}^{2+}$ ,  $\text{Cd}^{2+}$ ,  $\text{Cu}^{2+}$ ,  $\text{Mg}^{2+}$ ,  $\text{Pb}^{2+}$ ,  $\text{Ni}^{2+}$ ,  $\text{Na}^+$ ,  $\text{Li}^+$ , and  $\text{Al}^{3+}$ . Figure 4 shows the change in fluorescence intensity of N-GQDs in the presence of 25  $\mu\text{M}$  of different cations, including  $\text{Hg}^{2+}$  ions. The obtained result clearly showed that  $\text{Hg}^{2+}$  ions have the highest quenching effect compared to other ions. Therefore, it strongly proves that the synthesised N-GQDs were highly selective in the detection of  $\text{Hg}^{2+}$  ions.

### 3.6 Possible quenching mechanism of N-GQDs to $\text{Hg}^{2+}$ ions

A previous study commonly reported the static and dynamic quenching mechanism as a possible quenching mechanism

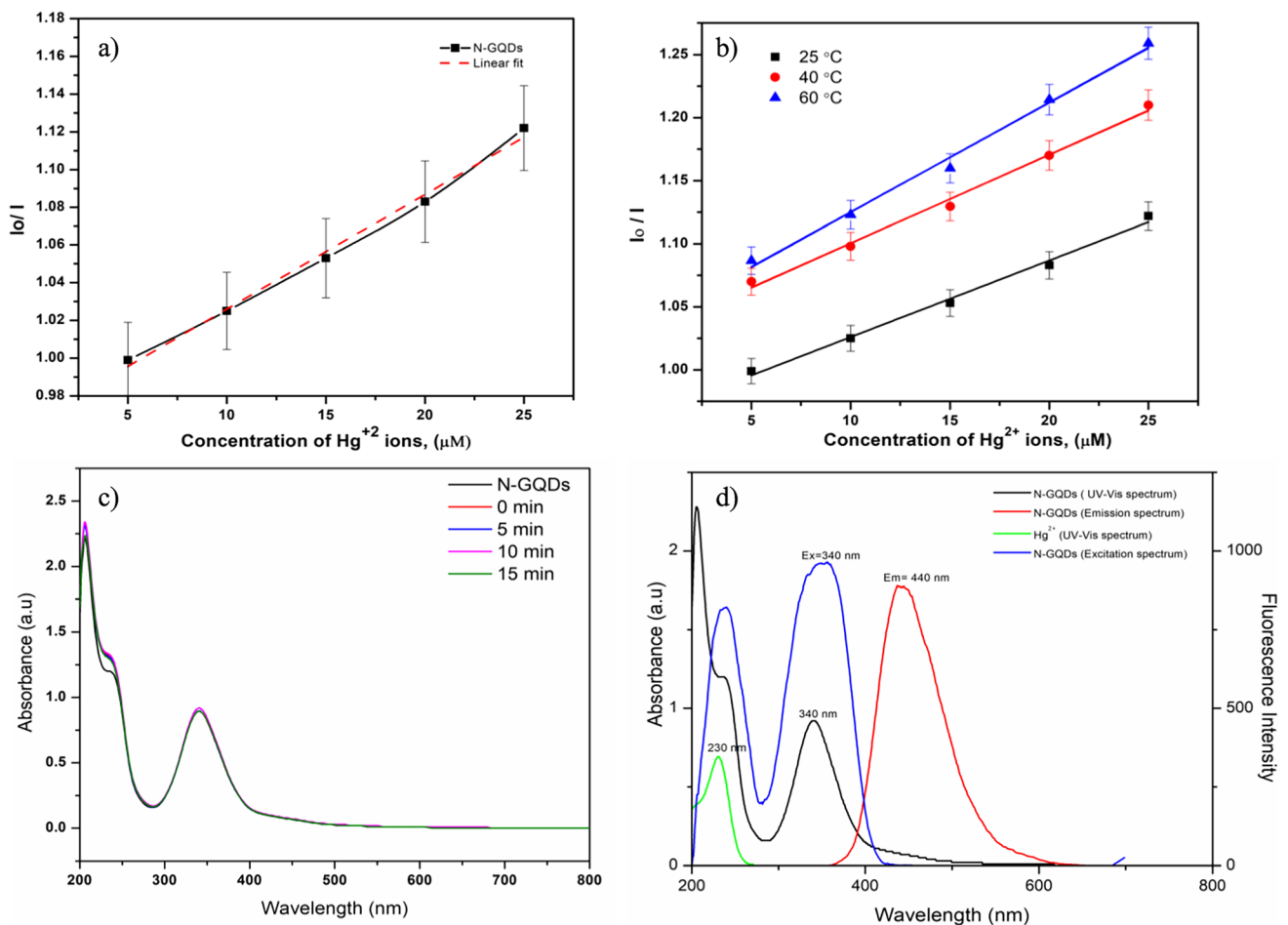


**Fig. 5** The Stern–Volmer plot for the interaction of  $\text{Hg}^{2+}$  ions and the N-GQDs (a) at different concentrations ( $n=3$ ) and (b) at different temperatures ( $n=3$ ). (c) The UV–Vis spectrum of N-GQDs and

N-GQDs spiked with  $\text{Hg}^{2+}$  ions at different incubation times. (d) Overlay of UV–Vis spectra (N-GQDs and  $\text{Hg}^{2+}$  ions) and the excitation and emission spectra of N-GQDs



that occurs between  $\text{Hg}^{2+}$  ions and the fluorescence N-GQDs [44]. Therefore, a Stern–Volmer plot for the interaction of  $\text{Hg}^{2+}$  ions and the N-GQDs for different concentrations has been plotted to determine the existence of static and dynamic quenching. The Stern–Volmer relationship was studied based on this equation:

$$I_0/I = 1 + K_{sv}[Q] \quad (4)$$

where,

$I_0$  Fluorescence emission intensity in absence of  $\text{Hg}^{2+}$  ions

$I$  Fluorescence emission intensity in presence of  $\text{Hg}^{2+}$  ions

$K_{sv}$  Stern–Volmer fluorescence quenching constant

$[Q]$  Concentration of the quencher ( $\text{Hg}^{2+}$  ions)

Based on the Stern–Volmer plot in Fig. 5a, the upward curve has been observed to correspond to the occurrence of both static and dynamic quenching between the interaction of  $\text{Hg}^{2+}$  ions and N-GQDs. Thus, for further confirmation, the studies on temperature-dependent quenching and the changes in UV–Vis spectra of N-GQDs and spiked  $\text{Hg}^{2+}$  ions in N-GQDs have been executed.

For the temperature-dependent study, a Stern–Volmer plot for the interaction of  $\text{Hg}^{2+}$  ions in N-GQDs at different temperatures has been plotted in Fig. 5b. It is clearly shown that the slope increased as the temperature rose, and it was confirmed that the quenching process was indicated by dynamic quenching. Moreover, from observation on the UV–Vis spectra of N-GQDs and spiked  $\text{Hg}^{2+}$  ions at different incubation time (0, 5, 10, and 15 min) in Fig. 5c, no significant difference was shown. Therefore, it is strongly supported that the possible quenching mechanism is dynamic quenching.

Besides, it was confirmed that there was no inner filter effect quenching mechanism that occurred in the quenching process because there is no overlay between the absorbance spectra of N-GQDs and  $\text{Hg}^{2+}$  ions and the fluorescence excitation and emission wavelength of N-GQDs as illustrated in Fig. 5d. Thus, dynamic quenching was proposed as the possible quenching mechanism in this work.

### 3.7 Detection of $\text{Hg}^{2+}$ ions in real water samples

Analysis of tap water and mineral water was conducted to evaluate the performance of the N-GQDs as a fluorescent probe for  $\text{Hg}^{2+}$  ions detection in real water samples. The calibration curve in Fig. 6 shows an excellent linear relationship between the fluorescence intensity ratios with the concentration of  $\text{Hg}^{2+}$  ions in distilled water. The linear equation obtained was  $y = 0.01236x + 1.0237$ , with correlation

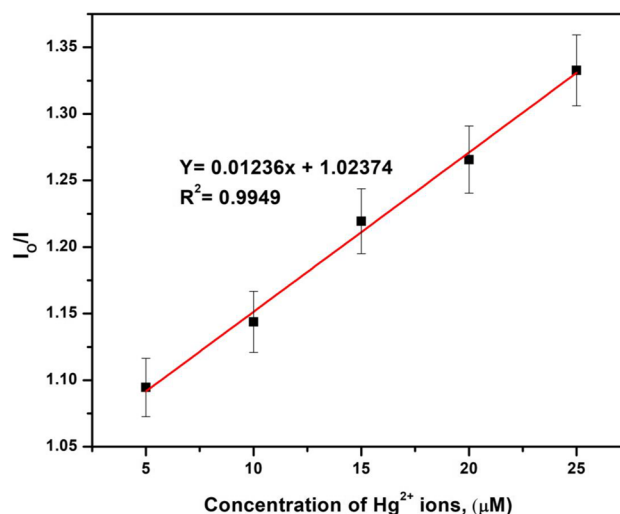


**Fig. 6** The calibration curve of the fluorescence intensity at 440 nm ( $I_0/I$ ) against  $\text{Hg}^{2+}$  ions concentration, where  $I$  and  $I_0$  are the fluorescence intensity in the presence and absence of  $\text{Hg}^{2+}$  ions, respectively ( $n = 3$ )

coefficient ( $R^2$ ) of 0.9949. This linear equation was used to calculate the  $\text{Hg}^{2+}$  ions present in tap and mineral water. From the calculation, the concentration of  $\text{Hg}^{2+}$  ions is negative for both water samples. Therefore, we can conclude that the  $\text{Hg}^{2+}$  ions were untraceable due to the low concentration present in tap and mineral water.

The percentage recovery was investigated after spiking 5, 15 and 25  $\mu\text{M}$  of  $\text{Hg}^{2+}$  ions into water samples. As a result in Table 2, tap and mineral water showed acceptable percentage recoveries between 99.00 and 100.70% in triplicate measurements. Therefore, the study method was reliable and had tremendous potential in real environment analysis.

**Table 2** Determination of  $\text{Hg}^{2+}$  ions concentration in tap and mineral water with its percentage recoveries ( $n = 3$ )

Samples	Spiked ( $\mu\text{M}$ )	Found ( $\mu\text{M}$ ) (Mean $\pm$ SD)	Recovery (%)	RSD (%)
Mineral water	-	N.D	-	-
	5	$5.02 \pm 0.10$	100.40	1.91
	15	$14.99 \pm 0.30$	99.90	1.99
	25	$25.18 \pm 0.15$	100.70	0.58
Tap water	-	N.D	-	-
	5	$5.00 \pm 0.39$	100.00	0.77
	15	$14.93 \pm 0.21$	99.50	1.39
	25	$25.07 \pm 0.24$	100.20	0.94

## 4 Conclusions

In this study, N-GQDs were prepared from citric acid and ethylenediamine as the carbon and nitrogen precursor by a facile hydrothermal process. The prepared N-GQDs with an average particle size of  $9.96 \pm 4.4$  nm was exhibited a bright blue fluorescence emission with a quantum yield of 36.23% and were evinced to have excitation-independent fluorescence emission at 440 nm with an excitation wavelength of 340 nm. Due to the enhancement on the chemical surface and fluorescence properties caused by doped nitrogen (N) atoms, the significant fluorescence quenching effect of N-GQDs in the presence of  $\text{Hg}^{2+}$  ions was detected after 15 min with 2.46  $\mu\text{M}$  and 7.45  $\mu\text{M}$  as the LOD and LOQ, respectively. Based on the intra-day and inter-day precision, it can be deduced that the detection of  $\text{Hg}^{2+}$  ions by N-GQDs has high accuracy because it has an RSD with acceptable percentage recovery. Furthermore, the quenching mechanism that occurred between the interaction of  $\text{Hg}^{2+}$  ions and N-GQDs was proved to be dynamic quenching. The as-synthesised N-GQDs also was found to have high selectivity towards  $\text{Hg}^{2+}$  ions compared to other metal ions and exhibit promising applications for  $\text{Hg}^{2+}$  ions detection in real water samples (tap and mineral water). In conclusion, N-GQDs produced using this hydrothermal synthesis can be further used as a fluorescent probe to detect  $\text{Hg}^{2+}$  ions in environment aqueous samples.

**Supplementary Information** The online version contains supplementary material available at <https://doi.org/10.1007/s42247-022-00365-z>.

**Acknowledgements** This work is financially supported by USM Research University Individual (RUI) Grant (1001/PKimia/8011086).

**Author contribution** H.L.L. and P.J. contributed to the study conception and design. Material preparation, data collection, and analysis were performed by A.S.A. and P.R. The first draft of the manuscript was written by A.S.A. and all authors commented on previous versions of the manuscript. All authors read and approved the final manuscript.

**Funding** This work is financially supported by USM Research University Individual (RUI) Grant (1001/PKimia/8011086).

## Declarations

**Competing interests** The authors declare no competing interests.

## References

- Z. Yan, X. Qu, Q. Niu, C. Tian, C. Fan, B. Ye, *Anal. Methods* **8**(7), 1565–1571 (2016). <https://doi.org/10.1039/x0xx00000x>
- R. Zhang, W. Chen, *Biosens. Bioelectron.* **55**, 83–90 (2013). <https://doi.org/10.1016/j.bios.2013.11.074>
- Y. Yang, X. Gou, J. Blecha, H. Cao, *Tetrahedron Lett.* **51**(26), 3422–3425 (2010). <https://doi.org/10.1016/j.tetlet.2010.04.100>
- F.S. Awad, K.M. AbouZied, W.M. Abou El-Maaty, A.M. El-Wakil, M. Samy El-Shall, *Arab. J. Chem.* **13**(1), 2659–2670 (2020). <https://doi.org/10.1016/j.arabj.2018.06.018>
- G. Azeh Engwa, P. Udoka Ferdinand, F. Nweke Nwalo, and M. N. IntechOpen, (2019). <https://doi.org/10.5772/intechopen.82511>
- S. Sharma, A. Bhattacharya, *Appl. Water Sci.* **7**(3), 1043–1067 (2017). <https://doi.org/10.1007/s13201-016-0455-7>
- P. Hajeb, S. Jinap, and A. Ismail, vol. 220. New York, NY: Springer New York, (2012). <https://doi.org/10.1007/978-1-4614-3414-6>
- H.H. Harris, I.J. Pickering, G.N. George, *Science* **301**(5637), 1203 (2003). <https://doi.org/10.1126/science.1085941>
- N.T.N. Anh, A.D. Chowdhury, R. Doong, *Sensors Actuators B Chem.* **252**, 1169–1178 (2017). <https://doi.org/10.1016/j.snb.2017.07.177>
- Y. Yang et al., *Mater. Res. Express* **6**(9)(2019). <https://doi.org/10.1088/2053-1591/ab3006>
- B. Passariello, M. Barbaro, S. Quaresima, A. Casciello, A. Marabini, *Microchem. J.* **54**(4), 348–354 (1996). <https://doi.org/10.1006/mchj.1996.0110>
- S. Zhu, B. Chen, M. He, T. Huang, B. Hu, *Talanta* **171**, 213–219 (2017). <https://doi.org/10.1016/j.talanta.2017.04.068>
- E. Yavuz, Ş Tokalioğlu, Ş Patat, *Microchem. J.* **142**(April), 85–93 (2018). <https://doi.org/10.1016/j.microc.2018.06.019>
- P. Hu et al., *Microchem. J.* **143**(August), 228–233 (2018). <https://doi.org/10.1016/j.microc.2018.08.013>
- C.F. Harrington, *TrAC - Trends Anal. Chem.* **19**(2–3), 167–179 (2000). [https://doi.org/10.1016/S0165-9936\(99\)00190-9](https://doi.org/10.1016/S0165-9936(99)00190-9)
- J. Duan, J. Zhan, *Sci. China Mater.* **58**(3), 223–240 (2015). <https://doi.org/10.1007/s40843-015-0031-8>
- A. Hasan et al., *Talanta* **215**(March), 120939 (2020). <https://doi.org/10.1016/j.talanta.2020.120939>
- Y. Lu et al., *Microchim. Acta* **183**(8), 2481–2489 (2016). <https://doi.org/10.1007/s00604-016-1886-4>
- H. Yang, Y. Xiong, P. Zhang, L. Su, F. Ye, *Anal. Methods* **7**(11), 4596–4601 (2015). <https://doi.org/10.1039/c5ay00633c>
- N.A. Azmi, S.H. Ahmad, S.C. Low, *RSC Adv.* **8**(1), 251–261 (2018). <https://doi.org/10.1039/c7ra11450h>
- Y. Chen et al., *Microchim. Acta* **177**(3–4), 341–348 (2012). <https://doi.org/10.1007/s00604-012-0777-6>
- M.J. Schnermann, *Nature* **551**(7679), 176–177 (2017). <https://doi.org/10.1038/nature24755>
- Y.L. Pak, Y. Wang, Q. Xu, *Coord. Chem. Rev.* **433**, 213745 (2021). <https://doi.org/10.1016/j.ccr.2020.213745>
- A. Salinas-Castillo et al., *Chem. Commun.* **49**(11), 1103–1105 (2013). <https://doi.org/10.1039/c2cc36450f>
- H. Li, Y. Zhang, X. Wang, Z. Gao, *Microchim. Acta* **160**(1–2), 119–123 (2008). <https://doi.org/10.1007/s00604-007-0816-x>
- Z. Qian et al., *RSC Adv.* **3**(34), 14571–14579 (2013). <https://doi.org/10.1039/c3ra42066c>
- X. Deng, Y. Feng, H. Li, Z. Du, Q. Teng, H. Wang, *Particuology* **41**, 94–100 (2018). <https://doi.org/10.1016/j.partic.2017.12.009>
- J. Ju, R. Zhang, S. He, W. Chen, *RSC Adv.* **4**(94), 52583–52589 (2014). <https://doi.org/10.1039/c4ra10601f>
- Y. Liu et al., *Microchim. Acta* **186**(3), 4–11 (2019). <https://doi.org/10.1007/s00604-019-3249-4>
- C. Hu, D. Liu, Y. Xiao, and L. Dai, vol. 28, no. 2. Elsevier B.V., pp. 121–132, (2018). <https://doi.org/10.1016/j.pnsc.2018.02.001>
- Y. Du, S. Guo, *Nanoscale* **8**(5), 2532–2543 (2016). <https://doi.org/10.1039/c5nr07579c>

32. H. Wang, T. Maiyalagan, X. Wang, *ACS Catal.* **2**(5), 781–794 (2012). <https://doi.org/10.1021/cs200652y>
33. Y. Ma et al., *Talanta* **196**(October 2018), 563–571 (2019). <https://doi.org/10.1016/j.talanta.2019.01.001>
34. R. Liu, D. Wu, X. Feng, K. Müllen, *J. Am. Chem. Soc.* **133**(39), 15221–15223 (2011). <https://doi.org/10.1021/ja204953k>
35. K. Li et al., *J. Mater. Chem. B* **5**(25), 4811–4826 (2017). <https://doi.org/10.1039/c7tb01073g>
36. A. Sharma, J. Das, *J. Nanobiotechnol.* **17**(1), 1–24 (2019). <https://doi.org/10.1186/s12951-019-0525-8>
37. P. Ramachandran, C.Y. Lee, R.A. Doong, C.E. Oon, N.T. Kim Thanh, H.L. Lee, *RSC Adv.* **10**(37), 21795–21805 (2020). <https://doi.org/10.1039/d0ra02907f>
38. T. Van Tam, N.B. Trung, H.R. Kim, J.S. Chung, W.M. Choi, *Sensors Actuators. B Chem.* **202**, 568–573 (2014). <https://doi.org/10.1016/j.snb.2014.05.045>
39. C. Zhao, Y. Jiao, J. Hua, J. Yang, Y. Yang, *J. Fluoresc.* **28**(1), 269–276 (2018). <https://doi.org/10.1007/s10895-017-2189-9>
40. F. Lu et al., *Int. J. Opt.* **2019**, 1–9 (2019). <https://doi.org/10.1155/2019/8724320>
41. F. Zu et al., *Microchim. Acta* **184**(7), 1899–1914 (2017). <https://doi.org/10.1007/s00604-017-2318-9>
42. D. Tang et al., *Nanoscale* **10**(18), 8477–8482 (2018). <https://doi.org/10.1039/c8nr01355a>
43. K. Nawara, J. Waluk, *Anal. Chem.* **91**(8), 5389–5394 (2019). <https://doi.org/10.1021/acs.analchem.9b00583>
44. O. Bunkoed, P. Kanatharana, *Luminescence* **30**(7), 1083–1089 (2015). <https://doi.org/10.1002/bio.2862>
45. L. Tang, R. Ji, X. Li, K.S. Teng, S.P. Lau, *J. Mater. Chem. C* **1**(32), 4908–4915 (2013). <https://doi.org/10.1039/c3tc30877d>
46. S. Krukowski, M. Karasiewicz, W. Kolodziejcki, *J. Food Drug Anal.* **25**(3), 717–722 (2017). <https://doi.org/10.1016/j.jfda.2017.01.009>
47. B. Zheng et al., *Nanophotonics* **6**(1), 259–267 (2017). <https://doi.org/10.1515/nanoph-2016-0102>
48. Y. Dong et al., *Angew. Chem. Int. Ed.* **52**(30), 7800–7804 (2013). <https://doi.org/10.1002/anie.201301114>
49. B. Shi, L. Zhang, C. Lan, J. Zhao, Y. Su, S. Zhao, *Talanta* **142**, 131–139 (2015). <https://doi.org/10.1016/j.talanta.2015.04.059>
50. Z. Wang et al., *Diam. Relat. Mater.* **104**(January), 107749 (2020). <https://doi.org/10.1016/j.diamond.2020.107749>
51. P. Tian, L. Tang, K.S. Teng, S.P. Lau, *Mater. Today Chem.* **10**, 221–258 (2018). <https://doi.org/10.1016/j.mtchem.2018.09.007>
52. Z. Yang et al., *Nano-Micro Lett.* **5**(4), 247–259 (2013). <https://doi.org/10.5101/nml.v5i4.p247-259>
53. M. Kaur, M. Kaur, V.K. Sharma, *Adv. Colloid Interface Sci.* **259**, 44–64 (2018). <https://doi.org/10.1016/j.cis.2018.07.001>
54. L. Li, T. Dong, *J. Mater. Chem. C* **6**(30), 7944–7970 (2018). <https://doi.org/10.1039/c7tc05878k>
55. H. Zhang et al., *Anal. Chem.* **86**(19), 9846–9852 (2014). <https://doi.org/10.1021/ac502446m>

**Publisher's note** Springer Nature remains neutral with regard to jurisdictional claims in published maps and institutional affiliations.